S. Lee, M. U. Demirci, and Clark T.-C. Nguyen, "A 10-MHz micromechanical resonator Pierce reference oscillator for communications," *Digest of Technical Papers*, the 11th Int. Conf. on Solid-State Sensors & Actuators (Transducers'01), Munich, Germany, June 10-14, 2001, pp. 1094-1097.

A 10-MHz Micromechanical Resonator Pierce Reference Oscillator for Communications

Seungbae Lee, Mustafa U. Demirci, and Clark T.-C. Nguyen
Center for Wireless Integrated Microsystems
Department of Electrical Engineering and Computer Science
University of Michigan, Ann Arbor, MI 48109-2122, U.S.A.

ABSTRACT

A modified Pierce circuit topology has been used to first demonstrate a 9.75 MHz μmechanical resonator reference oscillator, then to assess the ultimate frequency stability of such an oscillator via accurate measurement of its close-to-carrier phase noise, which seems to exhibit an unexpected $1/f^3$ dependence that limits the phase noise to –80 dBc at a 1 kHz offset from the carrier—a value that must be improved before use in most communications applications. Through theoretical analysis, this $1/f^3$ dependence seems to derive from aliasing of active circuit $1/f$ noise onto the carrier caused by nonlinearity in the capacitive transducer of the μmechanical resonator.

Keywords: resonator, high-*Q*, oscillator, stability

I. INTRODUCTION

Due to their ability to provide highly stable reference frequencies, high-*Q* oscillators serve an indispensable role in virtually all communication devices and instrumentation. To date, quartz crystals have been the preferred reference tanks used in such oscillators, mainly due to their exceptional *Q*'s (~50 000) and superb thermal and aging stability [1]. Unfortunately, however, their size and incompatibility with integrated circuits are inconsistent with present trends towards system-on-a-chip system implementations. For these applications, a fully integrated reference oscillator is desired, with its high-*Q* tank integrated on-chip.

Recent demonstrations of IC-compatible vibrating micromechanical ("μmechanical") resonators operating from HF to mid-VHF with *Q*'s in the tens of thousands [2] and reasonable temperature coefficients [3] have spurred great interest in the use of these devices as on-chip tanks for communications-grade oscillators. This paper details the design and implementation of such a reference oscillator utilizing a Pierce circuit topology and off-chip active circuitry. It begins with a discussion of design constraints unique to oscillators using high impedance μmechanical resonators, then proceeds to experimental evaluation of the oscillator, culminating in a phase noise measurement revealing an unexpectedly large $1/f^3$ noise component on the order of –80dBc/Hz at a 1 kHz offset from the carrier. The paper concludes with explanations for the observed noise behavior.

II. OSCILLATOR DESIGN

Figure 1 presents the complete circuit schematic utilized to instigate and sustain oscillation. Although it maintains the phase noise advantages [1] of the Pierce topology, this circuit differs somewhat from the conventional Pierce, as it uses two bipolar transistors instead of one in order to compensate for the large series motional resistance R_x of the clamped-clamped beam ("CC-beam") μmechanical resonator used to set the oscillation frequency. The additional transistor is needed not for additional gain, but rather for buffering, to insure that the overall loop phase shift ($=180^o + \phi_1 + \phi_2 + \phi_3$) shown in the conceptual circuit diagram of Fig .2 equals 0^o (or 360^o)—one of the fundamental conditions required for oscillation. In particular, interaction between the large R_x (~17.5 kΩ) of the μresonator and the surrounding capacitance tends to constrain ϕ_3 to smaller values than seen when a quartz crystal (with R_x~20 Ω) is used as the frequency setting element.

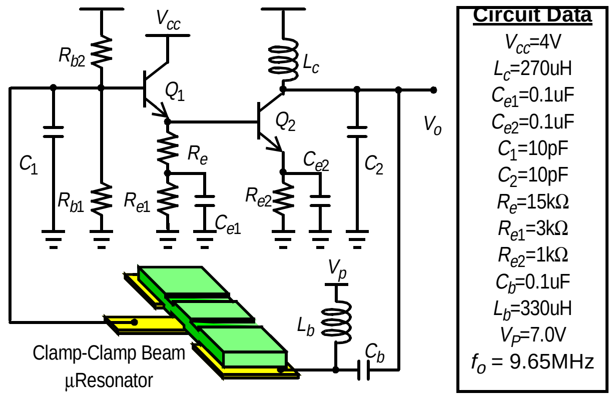

Fig. 1: Modified Pierce oscillator circuit utilizing a CC-beam μresonator tank.

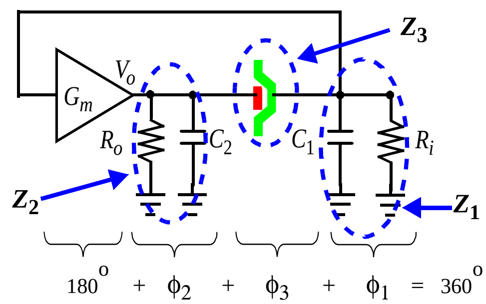

Fig. 2: Conceptual circuit schematic for the oscillator of Fig. 1.

The problem is perhaps best illustrated by obtaining an expression for the loop phase shift of the circuit, which is essentially equal to the phase of the loop gain expression. Referring to Fig. 2, the loop gain expression for the Pierce configuration can be written as

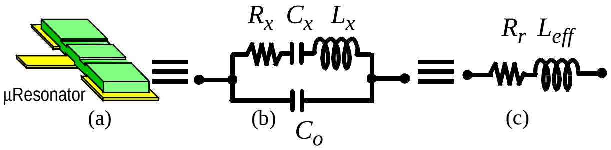

Fig. 3: A (a) µmechanical resonator with (b) its general electrical equivalent circuit and (c) its equivalent circuit when embedded in a Pierce oscillator at the oscillation frequency

$$G(j\omega_o) = G_m \frac{Z_1 \cdot Z_2}{Z_1 + Z_2 + Z_3}\text{, where} \tag{1}$$

$$Z_1(j\omega_o) = \frac{R_i}{1 + j\omega_o C_1 R_i}\ ,\ Z_2(j\omega_o) = \frac{R_o}{1 + j\omega_o C_2 R_o} \tag{2}$$

$$Z_3(j\omega_o) = j\omega_o L_{eff} + R_r\ , \tag{3}$$

where G_m is the steady-state transconductance amplifier gain, Z_1 and Z_2 are impedances indicated in Fig. 2, Z_3 is the impedance of CC-beam µmechanical resonator, and R_i and R_o are the input and output resistance of the sustaining amplifier, respectively. Here, it has been assumed that the resonator looks inductive at the frequency of oscillation ω_o (c.f., Fig. 3), where

$$L_{eff} = \frac{[\omega_o^2 C_{eff}(1 + C_o/C_{eff})^2]^{-1} - R_x^2 C_o}{1/(1 + C_o/C_{eff})^2 + \omega_o^2 R_x^2 C_o^2} \tag{4}$$

$$R_r \approx R_x = \frac{k_r}{\omega_o Q V_P^2 (\partial C/\partial x)^2}\ ,\ C_{eff} = \frac{C_1 C_2}{C_1 + C_2}, \tag{5}$$

and where k_r is the stiffness of the resonator beam at its midpoint; $(\partial C/\partial x)$ is the unit change in capacitance per displacement integrated over the electrode width, which goes as $1/d_o^4$, where d_o is the electrode-to-resonator gap; and expressions for the radian resonance frequency of the µmechanical resonator ω_o can be found in [2].

For proper start-up of oscillation, the loop gain magnitude and phase should satisfy

$$|G(j\omega_o)| = 1 \tag{6}$$

$$\angle G(j\omega_o) = 180^0 + \phi_1 + \phi_2 + \phi_3 = 360^0 \tag{7}$$

$$\phi_1 = \angle Z_1\ ,\ \phi_2 = \angle Z_2\ ,\ \phi_3 = \angle Z_3 \tag{8}$$

For a typical 10 MHz µmechanical resonator design, such as the one used for this work summarized in Table I, the value of R_x=17.5 kΩ often dictates a rather small value of L_{eff}=46 µH. With these element values, ϕ_3 often cannot exceed 50°—a value much smaller than normally achievable when a quartz crystal with a much smaller R_x=20 Ω is used. Thus, to satisfy the loop phase criterion of (7) when the example µmechanical resonator serves as the tank, ϕ_1 and ϕ_2 must combine to be at least 130° in order to instigate oscillation with this µmechanical resonator in the loop. If only one bipolar transistor is used to realize G_m, as is often done in Pierce oscillators referenced to quartz crystals, then as shown in Fig. 2, although its G_m would be large enough to satisfy (6), its R_i would not be large enough to generate enough $\phi_1 + \phi_2$ to make $\angle G(j\omega_o) = 0^0$. Thus, (7) would not be satisfied, and oscillations would not start-up.

To remedy this, a common-collector stage is inserted before the transconductance amplifier as shown in Fig. 1, to boost the R_i, and thus, generate a phase shift $\phi_1 + \phi_2$ large enough to satisfy (7). Once the above gain and phase conditions are met, oscillations start-up and grow until capacitive transducer non-linearity raises the R_x of the µmechanical resonator [4][5] to a value where the total loop gain is unity, at which point steady-state oscillation ensues. Note that this limiting mechanism based on resonator non-linearity is quite different from that exhibited by quartz crystal counterparts, which normally limit via transistor non-linearity. With this mechanism, for a given value of sustaining amplifier gain G_m, the amplitude of steady-state oscillation v_o is larger when the initial (i.e., start-up) value of R_x is smaller. In terms of power, the smaller the initial value of R_x, the larger the carrier output power.

III. µMECHANICAL RESONATOR DESIGN

Despite the fact that a Darlington sustaining amplifier makes possible the use of a large R_x µmechanical resonator tank circuit, there is still great incentive for reducing the value of R_x, since the oscillator power depends inversely upon its value. Oscillator power in turn determines the ultimate short-term stability of the oscillator, since the phase noise density goes inversely with the oscillator carrier power, as seen in the expression for phase noise $L\{f_m\}$

$$L\{f_m\} \approx \frac{kTF}{2V_o^2}\left[\frac{R_x}{Q_l^2}\right] \cdot \left[\frac{C_x}{C}\right]^2 \cdot \left[\frac{f_o}{f_m}\right]^2 \tag{9}$$

where f_m is the offset from the carrier frequency at which phase noise is being evaluated, V_o is the oscillator output voltage magnitude, C=C_1 is the external resonating capacitance, k is Boltzmann's constant, Q_l is the loaded quality factor of the tank, and F is the noise figure of the sustaining amplifier.

As governed by (5), R_x is most conveniently reduced by either raising the dc-bias voltage V_P, or by reducing the electrode-to-resonator gap spacing d_o. Given that the value of R_x goes as d_o^4, reducing d_o constitutes the most effective way to decrease R_x. However, the gap spacing d_o cannot be reduced indefinitely, since it sets the maximum displacement amplitude x_{max}, which in turn sets the maximum carrier amplitude, and thus, the maximum carrier power. In particular, if $x_{max} = d_o$, then an expression for maximum carrier voltage amplitude can be written

$$V_{omax} = \frac{d_o^3 k_r}{Q V_P \varepsilon_o W_r W_e} \tag{10}$$

where W_r is the width of the CC-beam, and W_e is the width of the electrode. The strategy for designing an optimal µmechanical resonator for maximum carrier power (hence, minimum phase noise) would then be to choose d_o and V_P such that R_x is reduced to the point where the oscillation amplitude $V_o = V_{o,max}$, as defined

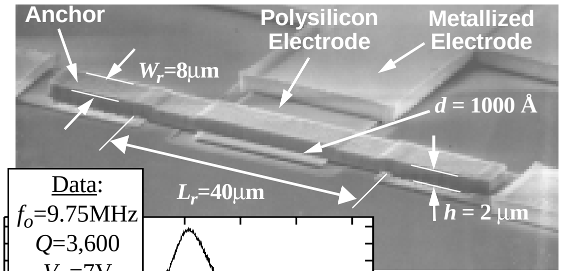

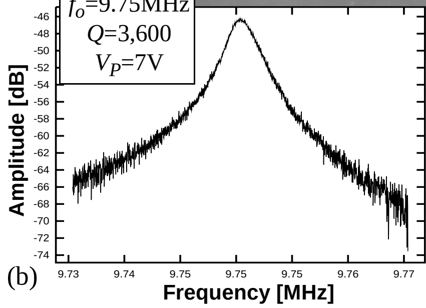

Fig. 4: (a) SEM and (b) measured frequency response for a ~10 MHz polysilicon vertical CC-beam μresonator.

Table I: 10 MHz CC-Beam μMechanical Resonator Pierce Oscillator Data

Parameter	Value	Units
μResonator Dimensions: L_r, W_r, h	40,8,2	μm
Electrode Width, W_e	20	μm
Electrode-to-Resonator Gap, d_o	1,000	Å
DC-Bias Voltage, V_P	7	V
Quality Factor, Q	3,600	—
Motional Inductance, L_x	0.836	H
Motional Capacitance, C_x	0.301	fF
Motional Resistance, R_x	17.5	kΩ
Static Capacitance, C_o	14.3	fF
Effective Inductance, L_{eff}	46	μH
Resistance at oscillation, R_r	17.6	kΩ

by (10).

IV. EXPERIMENTAL RESULTS

The oscillator circuit of Fig. 1 was realized using a 9.75 MHz CC-beam μmechanical resonator [7], together with off-chip, board-level electronic circuit components. Figures 4(a) and (b) present the SEM and measured frequency characteristic, respectively, for one of the 9.75 MHz resonators used for this work, while Table I summarizes its design. As discussed in Section III, pursuant to achieving a reasonable compromise between minimum series motional resistance R_x and maximum power handling capability, this μmechanical resonator features a width W_r of 8 μm and an electrode-to-resonator gap spacing d_o of 1000 Å. With V_P=7 V, the predicted series motional resistance is 17.5 kΩ, and the expected power threshold where the resonator vibration amplitude matches the electrode-to-resonator gap is 27 μW.

Figure 5 presents a photograph of the custom-made printed circuit board realizing the μmechanical Pierce oscillator. As shown, the resonator die is epoxied directly to the board to allow direct bonding of a μmechanical resonator to board leads connecting to surface mounted electronic circuit components. This approach greatly reduces parasitic capacitance, allowing the μmechanical devices to operate closer to theoretical prediction.

Fig. 5: Pierce oscillator test PCB board containing the circuit of Fig. 1, plus an output buffer to shield the oscillator loop from external loading.

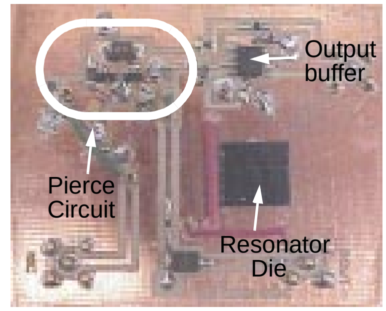

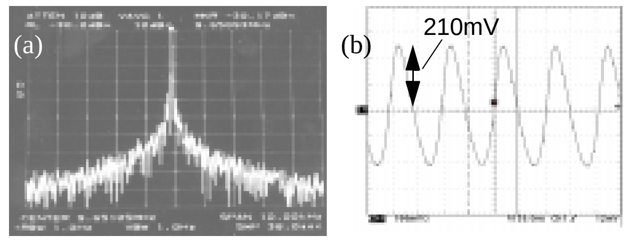

Fig. 6: (a) Measured Fourier spectrum for the modified Pierce oscillator, and (b) an oscilloscope waveform.

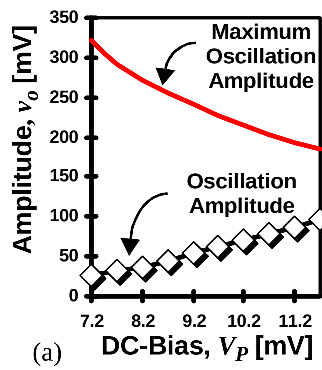

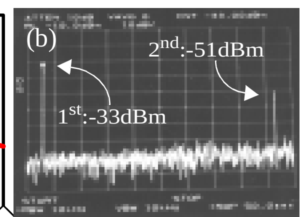

Fig. 7: (a) Oscillation amplitude vs. dc-bias V_P. (b) Measured Fourier spectrum showing a strong second harmonic oscillator output.

The oscillator was tested under 50 μTorr vacuum using a custom-built vacuum chamber with feedthroughs to external measurement instrumentation. Figure 6(a) presents the Fourier spectrum for this oscillator as measured by an HP 8561 Spectrum Analyzer, as well as an oscilloscope waveform in Fig. 6(b), showing an amplitude of 210 mV at the output buffer, which corresponds to ~100 mV at sustaining amplifier output, for operation with V_P=7 V. Consistent with resonator-based limiting predicted in Section III, the amplitude of the oscillator increased linearly with increases in the dc-bias voltage V_P. Figure 7 plots the oscillation amplitude v_o versus dc-bias V_P, clearly showing a linear relationship.

The slight distortion seen in waveform of Figure 6(b) arises from a rather large second harmonic peak, as shown in Fig. 7(b), which presents a Fourier spectrum of the oscillator output over a wider frequency range. This excessive second harmonic distortion peak arises from non-linearity in the μmechanical resonator's capacitive transducer, which generates harmonics in output current

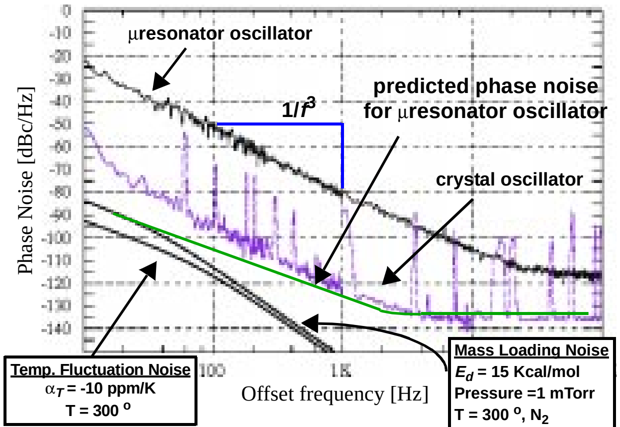

Fig. 8: Phase noise versus frequency offset from the carrier for a 9.75 MHz CC-Beam Pierce oscillator and a 10 MHz crystal version. Theoretical phase noise plots for the CC-beam oscillator are also included.

given by the expression

$$\begin{aligned} i_o(t) &= V_P\frac{\partial C(t)}{\partial t} = V_P C_o \frac{\partial}{\partial t}\left[\left(1+\frac{x\sin(\omega_o t)}{d_o}\right)^{-1}\right] \\ &\approx V_P C_o \omega_o \frac{x}{d_o}\left\{\underbrace{\left[1+\frac{3}{4}\left(\frac{x}{d_o}\right)^2\right]\sin\omega_o t}_{\text{Fundamental}} - \underbrace{\left[\left(\frac{x}{d_o}\right)+\left(\frac{x}{d_o}\right)^3\right]\cos(2\omega_o t)}_{2^{\text{nd}}\text{ harmonic}}\right\} \end{aligned} \tag{11}$$

For an output fundamental amplitude of 27 mV, (11) predicts a harmonic distortion factor [8] HD_2=-17 dB, which closely matches the HD_2=-18 dB extracted from the measured spectrum of Fig. 7(b).

Figure 8 finally presents a plot of phase noise density versus frequency offset from the 9.75 MHz carrier, measured using an HP E5500 Phase Noise Measurement system. The theoretical prediction using (9) is also included for comparison, as is the phase noise plot for an oscillator made using the same Pierce sustaining amplifier circuit, but with a quartz crystal (Q=7,000) replacing the µmechanical resonator. Evidently, the µresonator oscillator is not performing nearly as well as expected by (9).

Given the recent interest in "scaling-induced" physical noise mechanisms, such as adsorption-desorption noise (i.e., mass loading) or thermal fluctuation noise [9], that become more important as devices are scaled to achieve high frequencies, one might first suspect these noise sources as possible mechanisms. However, as shown in the predicted curves (using theory from [9]) for these noise mechanisms in Fig. 8, the dimensions of this 9.75 MHz resonator are large enough that the scaling-induced noise mechanisms should be insignificant even in comparison with noise predicted by (9), let alone the actual measured noise.

Closer inspection of Fig. 8 reveals that the slope of the phase noise curve at small frequency offsets is in fact not the $1/f^2$ predicted by (9) or by scaling-induced noise theories, but rather $1/f^3$, and it is this $1/f^3$ component that significantly degrades the short-term stability of this oscillator, limiting the phase noise to –80 dBc at a 1 kHz offset from the carrier. Although investigations into this are ongoing, initial analyses suggest the following possible mechanisms for this $1/f^3$ phase noise component:

(1) Non-linearity in the resonator capacitive transducer aliases $1/f$ electronic noise (e.g., from the sustaining amplifier) onto the carrier frequency, generating a $1/f^3$ component.

(2) $1/f$ noise associated with the dc-bias V_P on the resonator structure modulates the electrical stiffness k_e of the resonator [7], inducing a $1/f^3$ phase noise component.

(3) $1/f$ mechanical noise induces variations in the electrode-to-resonator gap spacing d_o, which then modulates the electrical stiffness k_e [7], generating a $1/f^3$ phase noise component.

Of the above, (1) is the most likely mechanism, since its expression for phase noise

$$L\{f_m\} = \frac{1}{4Q_l^2}\frac{1}{V_P^2}\left[\frac{1}{4}+\frac{Q_l^2}{k_{reff}^2}\frac{(\varepsilon_o A_o)^2}{d_o^6}\right]\cdot 2qK_1 I_B R_s^2 \cdot \frac{f_o^2}{f_m^3} \tag{12}$$

most closely matches the measured data. In (12), K_1 is the flicker noise coefficient for a bipolar transistor, I_B is its base current, and R_s is the transresistance gain of the sustaining amplifier. Assuming a $1/f$ noise corner of 50 kHz, I_B = 0.5mA, and R_s=14 kΩ, (12) gives -81 dBc/Hz @ 1 kHz for the oscillator of Fig. 8.

V. CONCLUSIONS

A 9.75 MHz µmechanical resonator reference oscillator has been demonstrated using a modified Pierce circuit topology in which a Darlington transconductance is used to sustain oscillation. Due to a larger degree of nonlinearity in the capacitively transduced µmechanical resonator tank, the behavior and performance of this oscillator differed sharply from that of its quartz crystal counterpart. In particular, whereas crystal oscillators limit via nonlinearity in the sustaining amplifier, this oscillator limits via nonlinearity in the resonator tank. In addition, although the µmechanical resonator used had a Q in the thousands, so should have exhibited a good $1/f^2$ noise performance, it instead showed a rather poor $1/f^3$ behavior generated largely by its own transducer nonlinearity. This effect has been analyzed and steps to remedy this noise mechanism are in progress.

Acknowledgment: This work was supported under DARPA Cooperative Agmt. No. F30602-97-2-0101.

References:

[1] R. J. Matthys, *Crystal Oscillator Circuits*. Wiley, 1983.
[2] K. Wang, *et al*., *IEEE/ASME JMEMS*, vol. 9, no. 3, pp. 347-360, Sept. 2000.
[3] W.-T. Hsu, *et al*., IEDM'00, pp. 399-402.
[4] C. T.-C. Nguyen, *et al*., *IEEE JSSC*, vol. 34, no. 4, pp. 440-455, April 1999.
[5] J. Cao, *et al*., *Transducers'99*, pp. 1826-1829.
[6] T. A. Roessig, *et al*., 1997 *Freq. Contr. Sym.*, pp. 778-782.
[7] F. D. Bannon III, *et al*., *IEEE JSSC*, vol. 35, no. 4, pp. 512-526, April 2000.
[8] D. O. Pederson, *et al*., *Analog Integrated Circuits for Communication*. Kluwer, 1991.
[9] J. R. Vig, *et al*., *IEEE UFFC*, vol. 46, no. 6, pp. 1558-1565, Nov. 1999.